Lattice Boltzmann simulation on particle suspensions in a two-dimensional symmetric stenotic artery

Huabing Li,[1,2,3] Haiping Fang,[1,2,*] Zhifang Lin,[2] ShiXiong Xu,[4] and Shiyi Chen[5]

[1]*Shanghai Institute of Applied Physics, Chinese Academy of Sciences, P.O. Box 800-204, Shanghai 201800, China*
[2]*Surface Laboratory and Department of Physics, Fudan University, Shanghai 200433, China*
[3]*Department of Computational Science and Applied Physics, Guilin University of Electronic Technology, Guilin 541004, China*
[4]*Department of Mechanics Engineering, Fudan University, Shanghai 200433, China*
[5]*Department of Mechanical Engineering, The Johns Hopkins University, Baltimore, Maryland 21218, USA*

The technique of lattice Boltzmann simulation has been applied to the study of two-dimensional particle suspensions through a modeled arterial stenosis. The stenosis model consists of two-side symmetric semicirculars in a planar channel with the width of the stenosis throat larger than d and less than $2d$, where d is the diameter of the particles. When only one particle is positioned off-centerline initially, the particle migrates off-centerline after passing the stenosis and the velocity at the stenosis throat is much larger than that in a flat tube. Only when two particles are positioned symmetrically to the centerline to a very high accuracy can the flow be blocked by two particles completely. A very small asymmetry will be amplified proximal to the stenosis throat in that one of the particles goes back to leave space to let the other particle passing the stenosis first so that the particles cannot be blocked. An evidence of attractive interactions between the particles as well as a particle and a proximal protuberance is observed when the asymmetry is very small and the width at the stenosis throat is between two critical values. The hematocrit distribution of the particles is studied by simulating multiparticle suspensions. It is found that the width of the stenosis throat has a significant influence on the hematocrit distribution of the particles in the flat tubes far from the stenosis.

I. INTRODUCTION

The flow and particle suspensions through stenosis vessels are of great interest in medical science [1–6]. Narrowing of blood flow, or stenosis, may cause a severe reduction in blood flow and red blood cell transportation. This reduction poses grave health risks and is a major cause of mortality and morbidity in the industrialized world. There are numerous papers on the study of the pulsatile flow in a mildly or severely stenotic artery. For example, Mittal *et al.* applied a large-eddy simulation to study pulsatile flow in a modeled stenosis [3]. The inclusion of particle suspensions in stenotic arteries adds complexity for theoretical and experimental analyses. The fluid dynamics of the flow and the moving of the particles are inextricably intertwined and both need to be understood. On the other hand, the solid-liquid suspensions in flat pipe flow have attracted much attention, both experimentally and numerically, in the past few decades. Early in 1961, Segré and Silberberg discovered experimentally that neutrally buoyant cylinders migrated laterally away both from the wall and the centerline and reached a certain lateral equilibrium position in pipe flow [7]. Fahraeus found that the hematocrit, the ratio of red blood cells to the total volume of a blood sample, in the small tube was smaller than that in the vessel [8]. Numerical simulations on particle suspensions in fluid flow are quite difficult and intensive due to the complexity of incorporating the hydrodynamic dynamics for liquid flow and the Newtonian dynamics for the particle moving through the solid-liquid interface. Feng *et al.* [9] used the infinite-element method to investigate the motion of a circular particle in a Couette and Poiseuille flow. Migliorini *et al.* [10] used a lattice Boltzmann approach to quantify the forces exerted on rolling leukocytes by red blood cells in "virtual blood vessels." Feng and Weinbaum [11] presented an axisymmetric model in which they treated the red blood cell surface as rigid but considered explicitly the build up in hydrodynamic pressure in the glycocalyx associated with dynamic compression of the layer. Das *et al.* [1] used a structural parameter k to characterize the average number of red blood cells in an aggregate to describe the hematocrit distribution while avoiding to simulate the moving of each red blood cell. This paper will concentrate on the particles moving through small stenosis tubes. We will use the lattice Boltzmann method [12–14].

The lattice Boltzmann method has been proved to be one of the most promising tools in the simulation of the solid-fluid two-phase flow. Based on the discrete Boltzmann equation [15] and inheriting the advantage of local nature of the computation, the lattice Boltzmann method has been proved to achieve second-order accuracy in the domain of the fluid, both theoretically and numerically [16]. Ladd [17] was the first to apply the lattice Boltzmann method to analyze a solid particle in a fluid. He proposed a modified bounce-back rule and a scheme to evaluate the hydrodynamic force exerted on the solid particles. Aidum *et al.* [18] attempted to improve Ladd's model by removing the fluid within the solid region so that they could handle a solid with density less than that of the fluid. Qi [19] applied the model to simulate the ellipse in nonzero Reynolds number flow. Behrend [20] analyzed

*Author to whom correspondence should be addressed. Email address: hpfang2000@yahoo.com

69 031919-1

the different boundary conditions based on the bounce-back rule and proposed a related bounce-back at the nodes. Raiskinmak *et al.* [21] applied the method to simulate non-spherical particles suspended in a shear flow. Both Ladd's and Aidum's models assumed a physical boundary located in the middle of the link between a solid node and a fluid node. The exact location of the physical boundary for the Behrend' model is more difficult to determine. Consequently, the hydrodynamic radius of a suspended particle differs from the input radius for those three models [21]. Noble and Torczynski proposed a lattice Boltzmann model to study the system with complex and moving geometries in which computational cells were partially filled with fluid [22]. Inamuro *et al.* [23] studied the neutrally buoyant circular cylinders in the flow between parallel walls. The force and torque were calculated by integrating stress tensor and momentum flux on a closed surface for a fixed radial distance $0.16D$ from the surface of the cylinder. Recently, Fang *et al.* [24,25] applied the lattice Boltzmann method to study the fluid flow in distensible blood vessels. Hoekstra *et al.* extended the method to harmonic flows. Within the range of Womersley numbers tested, the agreement between the simulations and the theory is good [26]. Hirabayashi *et al.* have performed lattice Boltzmann simulations for blood flow in a vessel deformed by the presence of an aneurysm [27].

Recently, we proposed a new lattice Boltzmann method to simulate two-dimensional moving particles in a Newtonian fluid [28]. Briefly, the boundary condition proposed by Filippova and Hanel [29,30] for the stationary complex geometry was incorporated with the Newtonian dynamics. The accuracy and robustness of this technique have been demonstrated by simulating sedimentation of a circular cylinder in a two-dimensional channel and comparing the simulation results with those obtained from a second-order finite-element method [28]. The method was successfully applied to study the sedimentation of a single charged circular cylinder in a two-dimensional channel in a Newtonian fluid [31]. In this paper, we will extend the method to simulate two-dimensional particle suspensions in symmetric stenotic arteries. The simulation shows that the stenosis not only increases the velocities of fluid and particles at the stenosis throat, but the particles may be blocked temporally when the width of the stenosis throat is smaller than two times the diameter of the particles. However, for rigid particles, only when the particles are positioned symmetrically to a very high accuracy can the symmetric stenosis be blocked completely. A little asymmetry will be amplified proximal to the stenosis throat in that one of the particles will go back to leave space to let the other particle pass the throat, implying that the stenosis throat cannot block the particles completed in a real system. Unexpected attractive interactions between the particles as well as a particle and a proximal protuberance are observed when the asymmetry is very small and the width at the stenosis throat is between two critical values. The hematocrit distribution of the particles is studied by simulating multiparticle suspensions.

The paper is organized as follows. In Sec. II we briefly describe the lattice Boltzmann method. Section III is devoted to a brief review of the boundary condition and hydrody-
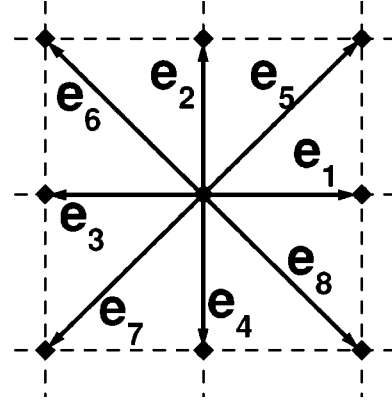
namics force exerted on the moving particles we used in the present paper. In Sec. IV, we present our simulation results. And finally, conclusion and discussion are presented in Sec. V.

FIG. 1. Basic cell for the two-dimensional ''nine-speed'' lattice Boltzmann model.

II. THE LATTICE BOLTZMANN MODEL

The Boltzmann equation with the single relaxation time approximation reads [32]

$$\frac{\partial f}{\partial t} + \boldsymbol{\zeta} \cdot \boldsymbol{\nabla} f = -\frac{1}{\lambda}[f - f^{(eq)}], \tag{1}$$

where $\boldsymbol{\zeta}$ is the particle velocity, $f^{(eq)}$ is the equilibrium distribution function, and λ is the relaxation time.

Discretizing Eq. (1) in the velocity space $\boldsymbol{\zeta}$ by using a finite set of velocities $\mathbf{e}_i$, we obtain [33,34]

$$\frac{\partial f_i}{\partial t} + \mathbf{e}_i \cdot \boldsymbol{\nabla} f_i = -\frac{1}{\lambda}[f_i - f_i^{(eq)}]. \tag{2}$$

In the model on a square lattice in two dimensions, $\mathbf{e}_0 = (0,0)$, $\mathbf{e}_i = (\cos \pi(i-1)/2, \sin \pi(i-1)/2)$, $i = 1,2,3,4$, and $\mathbf{e}_i = (\cos \pi(2i-1)/4, \sin \pi(2i-1)/4)$, for $i = 5,6,7,8$ are the nine possible velocity vectors as shown in Fig. 1, and the equilibrium distribution functions are of the form [33]

$$f_i^{eq} = \alpha_i \rho \left[1 + \frac{3}{c^2} \mathbf{e}_i \cdot \mathbf{u} + \frac{9}{2c^4}(\mathbf{e}_i \cdot \mathbf{u})^2 - \frac{3}{2c^2} u^2 \right], \tag{3}$$

for athermal fluids. In the equation, $\alpha_0 = 4/9$, $\alpha_1 = \alpha_2 = \alpha_3 = \alpha_4 = 1/9$, and $\alpha_5 = \alpha_6 = \alpha_7 = \alpha_8 = 1/36$, $c = \delta x/\delta t$ is the lattice speed, and δx and δt are the lattice constant and the time step, respectively. The density ρ and the velocity $\mathbf{u}$ are defined by

$$\rho = \sum_i f_i,$$

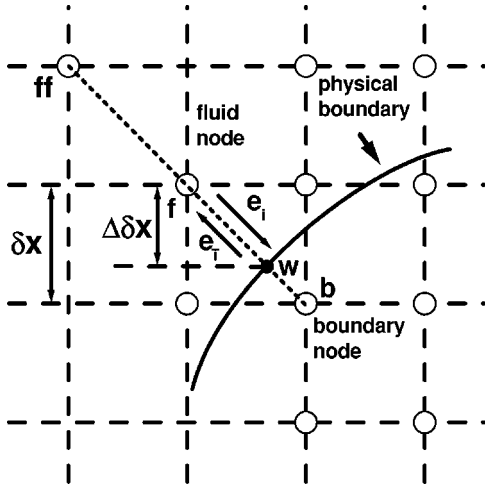$$\mathbf{u} = \sum_i f_i \mathbf{e}_i / \rho. \tag{4}$$

FIG. 2. Layout of the regularly spaced lattices and curved wall boundary.

The lattice Boltzmann equation [13,14] is obtained by further discretizing Eq. (2) in space **x** and time t as

$$f_i(\mathbf{x}+\delta x\mathbf{e}_i,t+\delta t)-f_i(\mathbf{x},t)=-\frac{1}{\tau}(f_i-f_i^{eq}),\qquad(5)$$

where $\tau=\lambda/\delta t$. The macroscopic equations can be obtained by a Chapman-Enskog procedure. The viscosity in the macroscopic equations is

$$\nu=\frac{(2\tau-1)}{6}c^2\delta t.\qquad(6)$$

In this paper, we set $\delta x=\delta t=c=1$.

III. BOUNDARY CONDITION FOR COMPLEX GEOMETRY

Filippova and Hanel [29] have presented their scheme for treating the boundary condition by considering a curved boundary lying between the lattice node of space $\Delta\,\delta x$ as shown in Fig. 2. The lattice nodes on the solid and fluid sides are denoted by $\mathbf{x}_b$ and $\mathbf{x}_f$, respectively. We assume

$$\mathbf{e}_i=\mathbf{x}_b-\mathbf{x}_f$$

and

$$\mathbf{e}_{\bar{i}}=-\mathbf{e}_i.$$

The filled small circle, marked by a letter w, at $\mathbf{x}_w$ is the intersection with the physical boundary on the link between $\mathbf{x}_b$ and $\mathbf{x}_f$. The fraction of an intersected link in the fluid is

$$\Delta=\frac{|\mathbf{x}_f-\mathbf{x}_w|}{|\mathbf{x}_f-\mathbf{x}_b|},\qquad0\leqslant\Delta\leqslant1.\qquad(7)$$

In the streaming step $f_{\bar{i}}(\mathbf{x}_f)$ is expected to be obtained by

$$f_{\bar{i}}(\mathbf{x}_f,t+\delta t)=f_{\bar{i}}(\mathbf{x}_b,t).\qquad(8)$$

However, the distribution function $f_{\bar{i}}(\mathbf{x}_b,t)$ at the boundary node b is unknown.

Fillipova and Hanel assumed the linear interpolation [29]

$$f_{\bar{i}}(\mathbf{x}_b,t)=(1-\chi)f_i(\mathbf{x}_f,t)+\chi f_i^{(*)}(\mathbf{x}_b,t)+6\alpha_i\mathbf{e}_{\bar{i}}\cdot\mathbf{u}_w,\quad(9)$$

where $\mathbf{u}_w=\mathbf{u}(\mathbf{x}_w,t)$ is the velocity at $\mathbf{x}_w$ and χ is a parameter. $f_i^{(*)}$ is a fictitious equilibrium distribution function given by

$$f_i^{(*)}(\mathbf{x}_b,t)=\alpha_i\rho[1+3\mathbf{e}_i\cdot\mathbf{u}_{bf}+\tfrac{9}{2}(\mathbf{e}_i\cdot\mathbf{u}_f)^2-\tfrac{3}{2}u_f^2],\quad(10)$$

where $\mathbf{u}_f=\mathbf{u}(\mathbf{x}_f,t)$ is the fluid velocity at the fluid node f shown in Fig. 2, $\mathbf{u}_{bf}$ is to be determined. Fillipova and Hanel proposed [29]

$$\mathbf{u}_{bf}=(\Delta-1)\mathbf{u}_f/\Delta+\mathbf{u}_w/\Delta\quad\text{and}\quad\chi=(2\Delta-1)/\tau$$

$$\text{for}\quad\Delta\geqslant\tfrac{1}{2}\qquad(11)$$

and

$$\mathbf{u}_{bf}=\mathbf{u}_f\quad\text{and}\quad\chi=(2\Delta-1)/(\tau-1)\quad\text{for}\ \Delta\leqslant\tfrac{1}{2},\quad(12)$$

to obtain a second-order scheme for the "slow flow." Mei *et al.* [30] improved the stability of the scheme at $\tau\approx1$ by replacing Eq. (12) by

$$\mathbf{u}_{bf}=\mathbf{u}_{ff}\quad\text{and}\quad\chi=(2\Delta-1)/(\tau-2)\quad\text{for}\ \Delta\leqslant\tfrac{1}{2}.\quad(13)$$

They have used the improved technique to test against several flow problems such as the two-dimensional channel flows with constant and oscillating pressure gradients, flows due to an impulsively started wall, lid-driven square cavity flows, and flows over a column of circular cylinders to demonstrate its accuracy and robustness [30].

For each *relevant* direction $\mathbf{e}_i$ from a fluid node to a boundary node, the solid boundary obtained an amount of momentum $f_i(\mathbf{x}_f,t_+)\mathbf{e}_i-f_{\bar{i}}(\mathbf{x}_b,t)\mathbf{e}_{\bar{i}}$ where the first term is due to a fraction of particles $f_i(\mathbf{x}_f,t_+)$ colliding on the boundary and the second term comes from a fraction of particles $f_{\bar{i}}(\mathbf{x}_b,t)$ bouncing back from the boundary in a time step. Consequently, the hydrodynamic force exerted on the solid particle at time t along this direction is

$$\mathbf{F}(\mathbf{x}_b)=[f_i(\mathbf{x}_f,t_+)+f_{\bar{i}}(\mathbf{x}_b,t)]\mathbf{e}_i,\qquad(14)$$

where t_+ is the postcollision time, and $f_{\bar{i}}(\mathbf{x}_b,t)$ is obtained from Eq. (9). The particle force $\mathbf{F}_T$ and torque $\mathbf{T}_T$ acting on the solid particle are obtained as

$$\mathbf{F}_T=\sum\mathbf{F}(\mathbf{x}_b)\qquad(15)$$

and

$$\mathbf{T}_T=\sum(\mathbf{x}_b-\mathbf{R})\times\mathbf{F}(\mathbf{x}_b),\qquad(16)$$

where **R** is the center of mass of the solid particle. The summation runs over all the relevant directions of the boundary nodes.

The translation of the center of mass of each particle is updated at each Newtonian dynamics time step by using a so-called half-step "leap-frog" scheme [37–39]. The scheme is written as

$$\mathbf{V}(t + \tfrac{1}{2}\delta t) = \mathbf{V}(t - \tfrac{1}{2}\delta t) + \delta t \mathbf{F}_T(t)/M, \qquad (17)$$

$$\mathbf{R}(t + \delta t) = \mathbf{R}(t) + \delta t \mathbf{V}(t - \tfrac{1}{2}\delta t) + \delta t^2 \mathbf{F}_T(t)/M, \quad (18)$$

where $\mathbf{V}$ is the velocity of the center of mass of the solid particle, and M is the mass of the solid particle. The rotations of the particles are updated in a similar way.

Due to the moving of the particles, some fluid nodes can be covered by the moving solid particles, the fluids at these nodes will be removed from the system. On the other hand, when a fluid node previously occupied by a solid particle is recovered, the fluid density at this newly created node is assumed to be the average of the extrapolated values from a *second-order extrapolation scheme* of all the possible directions [28,35]. In Ref. [25] we have shown that the mass is conserved approximately at boundaries.

It is clear that both the boundary condition for the complex geometry and the Newtonian dynamics for the moving particles achieve second-order accuracy. The accuracy of this lattice Boltzmann scheme has been demonstrated by simulating the sedimentation of a cylinder circular in a vertical tube and comparing the simulation results with those obtained from a second-order finite-element scheme [28]. The method has been successfully applied to the study of the sedimentation of a single charged circular cylinder in a two-dimensional channel in a Newtonian fluid [31].

When there are more than one particle in a tube, the lattice Boltzmann method breaks down when particles are closer than some critical separations. Introduction of a lubrication force is one of the solutions to solve this problem [40,41]. Lubrication forces are significant only when in close proximity. In this paper, only the normal lubrication forces between two particles F_N^{lub} are added. Yuan and Ball [41] proposed the lubrication forces between two circular particles with same radius as

$$F_N^{lub} = -\frac{3}{2}\pi\eta\frac{R}{s}\sqrt{\frac{R}{s}}(v_a^N - v_b^N), \qquad (19)$$

where s is the fringe-to-fringe gap, v_a^N and v_b^N are the velocities along the normal direction of the two particles, respectively. When the radii of two particles are different, which are R_a and R_b separately, this formula can be extended to the form [42]

$$F_N^{lub} = -\frac{3}{2}\pi\eta\frac{1}{s}\frac{2R_aR_b}{R_a+R_b}\sqrt{\frac{1}{s}\frac{2R_aR_b}{R_a+R_b}}(v_a^N - v_b^N). \quad (20)$$

Ladd [40] suggested that $1/s$ in Eq. (20) is replaced with $1/s - 1/\Delta_c$, Δ_c is the cutoff for the added lubrication force; for gaps s larger than Δ_c the lattice Boltzmann model captures the full hydrodynamic interactions between the particles, and $\mathbf{F}_N^{lub} = 0$. $\Delta_c = 1$ in the present simulation.
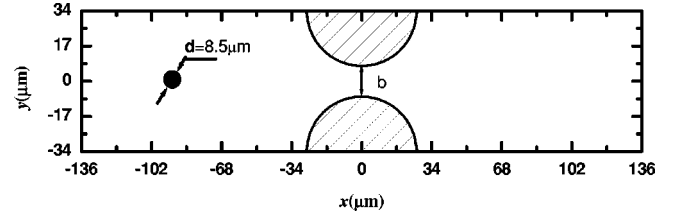

FIG. 3. Schematic diagram of the planar channel with stenosis. The length L and width w of the channel are 272 μm and 68 μm, respectively. $d = 8.5$ μm is the diameter of the circular particle suspensions. The upper (lower) protuberance is a semicircle, centered at $x = 0$ on the upper (lower) boundary with radius determined by the width of the stenosis throat b.

IV. SIMULATION AND RESULTS

The system is a two-dimensional rigid planar channel of length L and width w as shown in Fig. 3. $w = 8d$ and $L = 32d$, where $d = 8.5$ μm is the diameter of the circular particle suspensions, which approximately equals the diameter of human red blood cells. The stenosis is created by adding two symmetric protuberances inside the vessel. The upper (lower) protuberance is a semicircle, centered at $x = 0$ on the upper (lower) boundary with radius determined by the width of the stenosis throat b. In this paper $d < b < 2d$. The densities of both fluid and particles are 1 g/cm^3 and the kinematic viscosity of the fluid flow is $\nu = 0.01$ cm^2/s, corresponding to the water at 20 °C. The pressure difference between the inlet and outlet is $\Delta p = 541$ Pa, comparable to that in the arteriole of the cat mesentery (see Table 5.5:2 of Ref. [6]). A pressure boundary condition, proposed by Zou and He [36], is applied at the inlet and outlet. Initially the distribution functions at all the fluid nodes are set to be the equilibrium distribution functions with zero velocity except for those at inlet or outlet. The particles are positioned $8d$ left to the stenosis throat, keeping motionless at their initial positions in the first 5000 time steps. From $t = 5000$ time steps the particles are free to move according to the hydrodynamic forces and torques acting on them. In the simulation, $\tau = 0.75$. The radius of the particles is 7.001 lattice units which is large enough to obtain accurate results [28]. Consequently, each lattice unit corresponds to 8.5 μm/7.001/2 = 0.607 μm. The typical velocity of the particles, u_t, in the flat tube is about 1.5 cm/s, comparable to the velocity of the red blood cells in a cat artery with a diameter 56 μm (see, Fig. 5.3:1 of Ref. [6]). The particle Reynolds number is defined by Re$_p = du_p/\nu$, where u_p is the velocity of a particle. Re$_p \approx 0.13$ in the flat tube.

A. Motion of a single circular particle in a channel with the stenosis throat $b = 1.75d$

If the initial position of a particle falls on the centerline of the channel, the particle always stays on the centerline and the velocity at stenosis throat is much larger than that in the flat tube as shown in Fig. 4. The case is more complex when the particle is positioned away from the centerline initially. The snapshots of the positions and orientations of the particle are displayed in Fig. 5 for the initial position of the particle
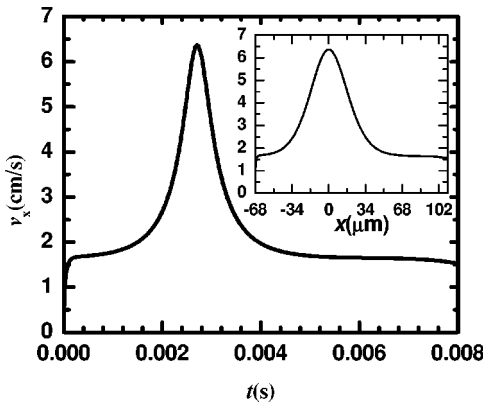
FIG. 4. The x component of the velocity of a particle passing through a channel with stenosis with respect to the time t and x value of the trajectory (inset). The initial position falls on the centerline.

$2d$ above the centerline. Near the protuberance the particle moves to the centerline of the tube. However, the particle never arrives at the centerline. After passing the stenosis, the particle migrates to the same direction of the initial position, i.e., the particle migrates up since the initial position of the particle is above the centerline. This is consistent with the Segré-Silberberg effect [7] observed in flat pipe flow that neutrally buoyant cylinders migrate laterally away from both the wall and the centerline and reach a certain lateral equilibrium position. Figure 6 shows the velocity and angular velocity of the particle with respect to t and x. The x component of the velocity at stenosis throat is about five times of that in the flat tube. The y component of the velocity changes its direction from upstream to downstream of the stenosis. The angular velocity at the throat is not so smooth as that of the x or y component of the velocity. This results from that the particle sometimes touches the upper protuberance near the stenosis throat like a skier. When the particle touches the upper protuberance, there is friction on the surface between the upper protuberance and the particle. Although the friction is very small, it gives a relatively large torque since it acts on the surface of the particle and is perpendicular to the connection line between the contact point and the center of the particle. Figure 7 shows the streamline in the tube.
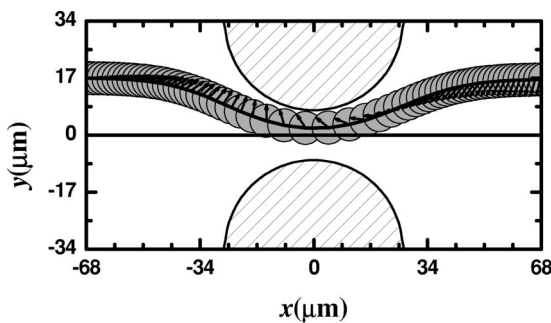
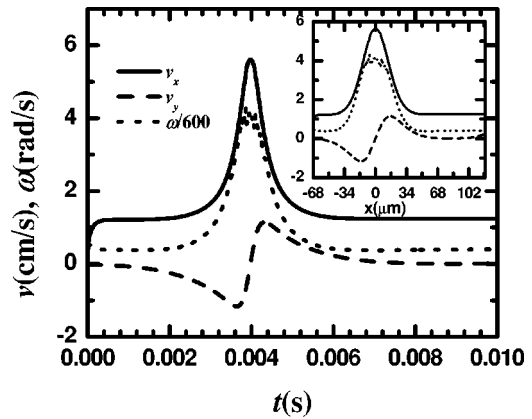FIG. 6. The velocity and angular velocity of the particle shown in Fig. 5 with respect to the time t and x value of the trajectory (inset).

B. Motion of two circular cylinders in a channel with $b = 1.75d$

Figure 8 displays the trajectories of two planar circular particles symmetric to the centerline initially. Their velocities and angular velocities are shown in Fig. 9. The x components of the velocities for both particles are consistent and merge into one. Since the width at the stenosis throat is only $1.75d$ and the particles are undeformable, it is impossible for two circular particles to pass the throat simultaneously. The particles stop near the throat and all the velocities and angular velocities vanish. It should be noted that there is a crucial difference between the two-dimensional circular particles and three-dimensional spheres passing a stenosis channel. In the two-dimensional case, not only both the particles are at rest, but the velocities at all fluid nodes vanish after the throat is completely blocked by particles. However, there is space for the fluid to flow even if the particles are blocked by the stenosis throat in three dimensions. The phenomena are more interesting when two planar circular particles are positioned asymmetric to the centerline initially. Figure 10(a) displays the snapshots. Initially the upper particle is positioned $2d + \varsigma$ above the centerline and the lower particle is positioned $2d$ below the centerline, where $\varsigma = d/4000$. Unlike that shown in Fig. 8, the particles will not block the throat completely due to the very small asymmetry. The par-

FIG. 5. The snapshots of the positions and orientations of a particle with the initial position $2d$ above the centerline.
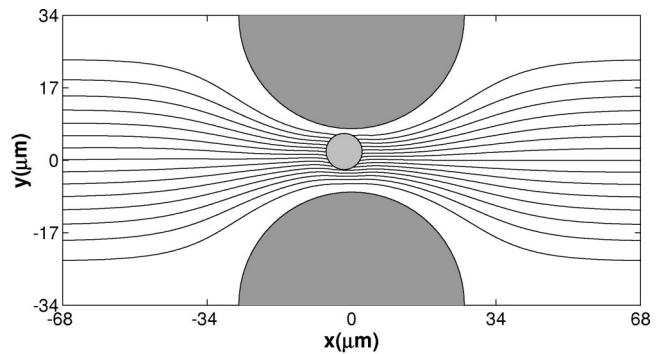
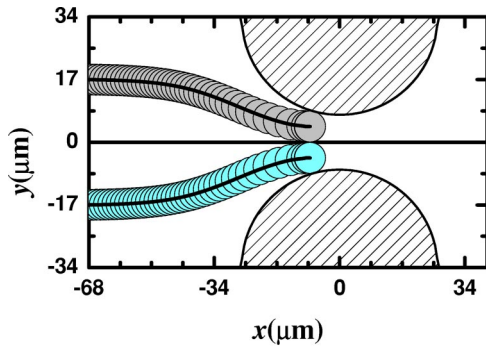FIG. 7. The streamline together with the circular particle in the stenosis tube.

FIG. 8. The snapshots of the positions of two circular particles with the initial position symmetric to the centerline with $b = 1.75d$.

ticles move almost symmetrically for the snapshots numbered 1 to 9. From the snapshot marked 9, the asymmetry amplifies. The lower particle still moves forward while the upper particle will stop and then move back, leaving space to let the lower particle pass the throat as the kink shown in the enlarged part of the trajectory displayed in Fig. 10(b). Once the space is enough to let the lower particle pass the stenosis throat, the upper particle changes its moving direction again and follows the lower particle. In Fig. 11 we show the streamline when the upper particle begins to move back. It is clear that both particles rotate.
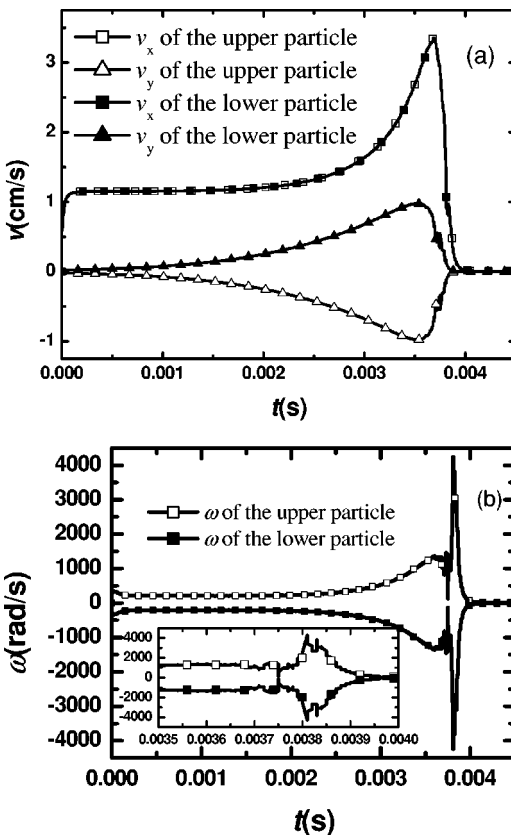

FIG. 9. The time-dependent velocity (a) and angular velocity (b) of the particle shown in Fig. 8. The inset is part of the enlarged figure.
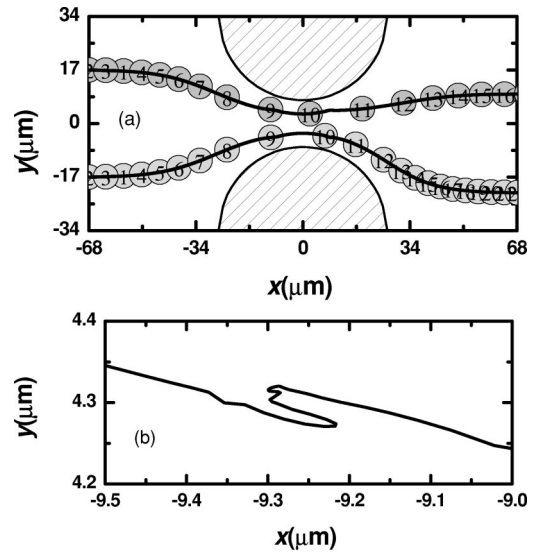

FIG. 10. The snapshots and the trajectories of two circular particles with the initial position asymmetric to the centerline with asymmetry $d/4000$ and $b = 1.75d$. The time interval between the snapshots is 0.001 06 s. The enlarged part of the trajectory of the upper particle shows that the particle moves back first, leaving space to let the lower particle passing the throat first.

C. Motion of two circular cylinders in a channel with $b \neq 1.75d$

Figure 12 displays the snapshots of two circular cylinders in a channel with $b = 1.5d$. Initially the upper particle is positioned $2d + \varsigma$ above the centerline and the lower particle is positioned $2d$ below the centerline, where $\varsigma = d/4000$. Unlike that for $b = 1.75d$, both particles move upward downstream of the stenosis, suggesting an evidence of attractive forces between two particles after the two particles pass the stenosis throat. Grier *et al.* [43] studied the influence of a glass wall on the interaction between small charged polystyrene particles of 0.652 μm and found some long distance attractive interaction between the particles 3–5 μm apart when they were close to the wall ($\sim$2.5 μm) while there was only a repulsive force when they were away from the wall ($\sim$9.5 μm). In our simulation, there are no charges on the particles and the diameter is 8.5 μm. In Fig. 13 we show the
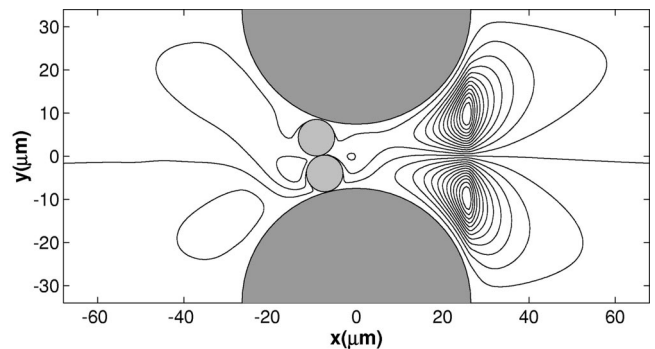

FIG. 11. The streamline together with the circular particles proximal to the stenosis throat. The streamline shows that both particles rotate.
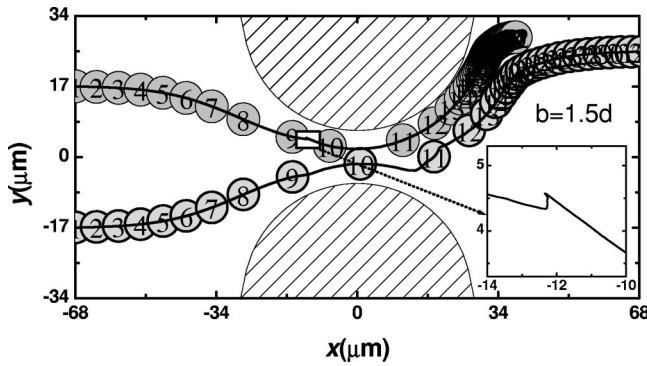
FIG. 12. The snapshots and the trajectories of two circular particles with the initial position asymmetric to the centerline with asymmetry $d/4000$ and $b=1.5d$. The time interval between the snapshots is 0.000 046 s. The enlarged part of the trajectory of the upper particle.

fringe-to-fringe distances between the two particles, the upper particle and the upper protuberance, and the lower particle and the lower protuberance. The fringe-to-fringe distance between the lower particle and the lower protuberance has a minimal value at $x=-10$ and increased gradually. The distance is larger than 1 μm at $x=13$ μm. However, the distance between two particles stays very small from $x=-12$ to 25 μm. From $x=10$ to 25 μm the distance between the upper particle and the upper protuberance is also very small. If the asymmetry ς initially is sufficiently large, the attractive forces between two particles are weak enough that the lower particle moves downwards after passing the stenosis, as displayed in Fig. 14 for ς$=d/40$.

Numerical simulations show that there are two critical values b_{c0} and b_c. Both particles move upward downstream for $b_{c0} \lesssim b \lesssim b_c$ while the lower particle moves downward for $d < b < b_{c0}$ or $b > b_c$. It is found that $b_{c0} \approx 1.26d$ and $b_c \approx 1.65d$ numerically. To further understand the behavior of the particles, the velocities of both particles for different b at $x=15$ μm downstream are shown in Fig. 15. The values of
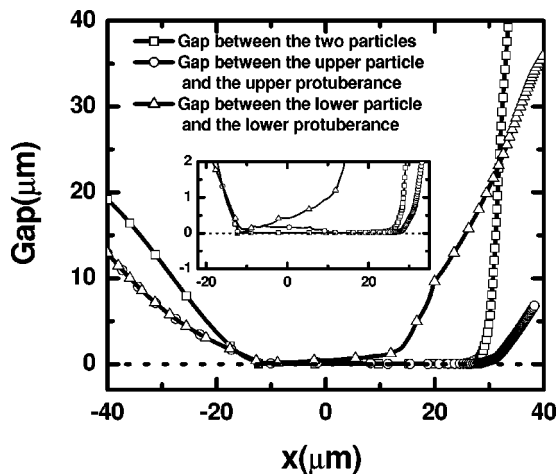

FIG. 13. The fringe-to-fringe distances between the two particles, the upper particle and the upper protuberance, and the lower particle with the lower protuberance for ς$=d/4000$.
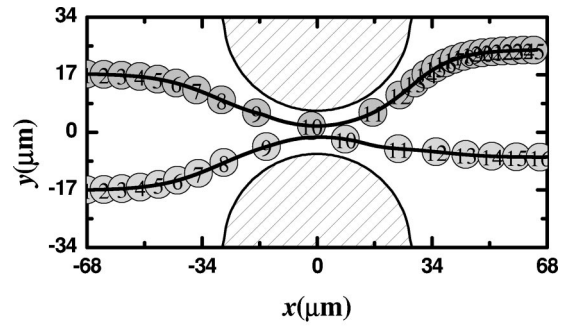

FIG. 14. The snapshots of two circular particles positioned initially asymmetrically with ς$=d/40$.

b_{c0} and b_c can also be found in the figure at which $v_y \approx 0$. Numerically we cannot distinguish whether $v_y = 0$ occurs exactly at $b = b_{c0}$ or b_c due to the interaction of two particles through fluid.

The suggested attractive force between two particles around $b=1.5d$ may be particular to two-dimensional systems. We have performed numerical simulations on a quasi-two-dimensional system [44]. Explicitly, the numerical simulations are performed in three dimensions. The particles are disks $0.171d$ thick in z direction, where d is the diameter of the disks. The length of the channel in z direction is $0.286d$ and periodic boundary condition is applied in z direction.
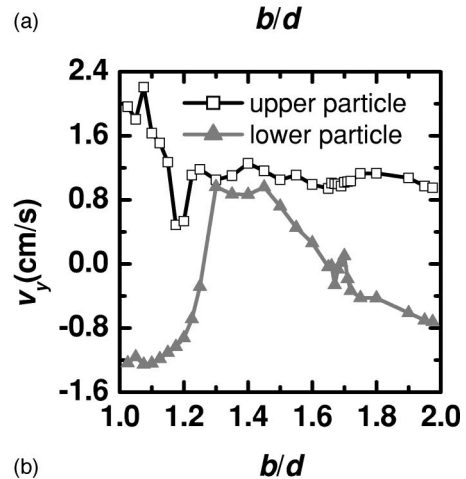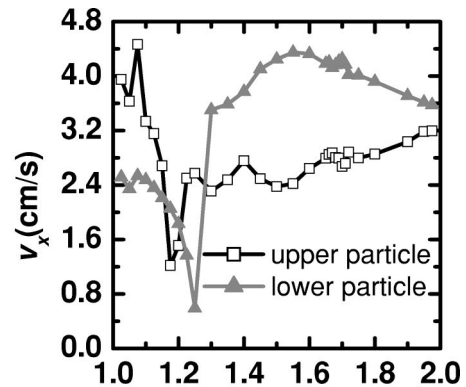

(a)

(b)

FIG. 15. The velocities of both particles for different b at $x=15$ μm downstream.
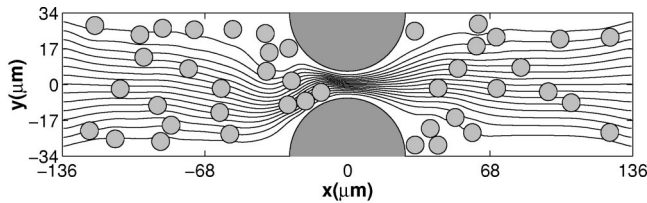
FIG. 16. A snapshot of many circular particles in a stenosis tube together with the streamline.

The two-dimensional projection of the quasi-two-dimensional system is the same as the two-dimensional system described in the present paper. The attractive interactions between the particles as observed in Fig. 12 almost disappear. The lower particle is always below the centerline.

In two-dimensional models, as the fluid flow is much more confined, interaction is significantly enhanced between particles when they depart from each other, giving rise to the observable phenomenon as shown in Fig. 12. In three-dimensional cases, fluid can flow from the z direction into the space between particles, leading to a much weaker (if any) attractive interaction between the particles. As a result, the lower particle always goes below center line, instead of following the upper one.

D. Motion of more circular particles in a channel with stenosis

Figure 16 shows a typical snapshot together with the streamline for $b=1.5d$. The hematocrit of the injected fluid is 0.2 and the particles from the inlet are positioned randomly along y direction. The average velocity of the particles in the flat tube is 0.95 cm/s, which corresponds to the Reynolds number 0.08. Ample experimental evidence suggests that hematocrit distribution in the microvaculature is not uniform: Red blood cells tend to concentrate near the center of the vessel [1]. The heterogeneous distribution of the particles in stenosis vessels is more complex. We define a quantity Φ at x to characterize this behavior:

$$\Phi(x) = \left\langle \frac{\xi}{\Xi(x)-r} - 0.5 \right\rangle, \tag{21}$$

where $\Xi(x)$ is half of the width of space of the tube at x, ξ is the distance between the center of any particle at x and the centerline, and r is the radius of the particles. In flat tubes, $\Phi=0$ if the particles are uniformly distributed in the tube as the solid line shown in Fig. 17, while $\Phi=-0.5$ and $\Phi=0.5$ correspond, respectively, to the cases that all particles fall on the centerline and touch the boundaries. In the flat tube, $\Phi<0$ implies that the particles tend to concentrate near the centerline of the vessel, and $\Phi>0$ corresponds to that the particles incline to gather close to the vessel walls. The simulation results are shown in Fig. 17. It is found that $\Phi>0$ for $b=1.5d$ and $\Phi<0$ for $b=1.75d$ in the flat tube far away from the stenosis. Similar to that discussed in Sec. IV B on the behavior of two particles downstream, there are two critical value $b_{c\Phi0}$ and $b_{c\Phi}$. $\Phi>0$ when $b_{c\Phi0}<b<b_{c\Phi}$ and vice versa in the flat tube far away from the stenosis, implying that the width of the stenosis throat has significant influence
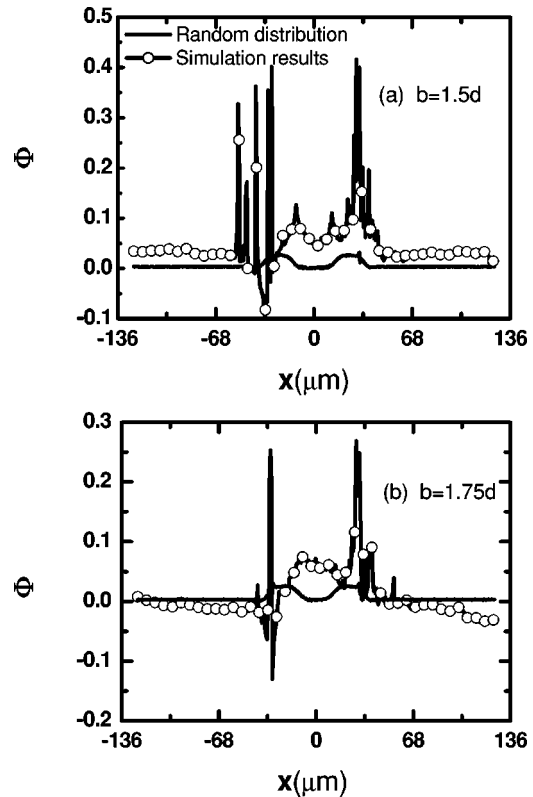

FIG. 17. Φ characterizing the distribution of the particles in the tube for (a) $b=1.5d$ and (b) $b=1.75d$. The irregular peaks result from the particles staying almost at rest at the corners between the flat tube and the protuberances.

on the hematocrit distribution of the particles in the flat tubes. Numerically we find that $b_{c\Phi0}\approx b_{c0}$ and $b_{c\Phi}\approx b_c$. This behavior is also consistent with the observation that red blood cells tend to concentrate near the centerline of the vessel in flat tubes [1]. Both the values of Φ for $b=1.5d$ and $b=1.75d$ at the stenosis throat are greater than that of a random distribution as shown in the solid line in Fig. 17, indicating a tendency of particle gathering near the wall. The peaks at $x\approx\pm35$ μm result from the particles staying almost at rest at the corners between the flat tube and the protuberances.

V. CONCLUSION AND DISCUSSION

We have applied the lattice Boltzmann method to the study of particle suspensions through a modeled arterial stenosis. The stenosis not only increases the velocities of fluid and particles at the stenosis throat, but also the particles may be blocked temporally when the width of the stenosis throat b is larger than d and smaller than $2d$, where d is the diameter of the particles. However, for rigid particles, only when the particles are positioned symmetrically to a very high accuracy can the symmetric stenosis be blocked completely. A very small asymmetry will be amplified proximal to the stenosis throat in that one of the particles will go back to leave space to let the other particles pass the throat, implying that the stenosis throat cannot be completely blocked by particles in a real system. This is quite different from the

jamming phenomena of granular flow in a hopper [45]. Moreover, an evidence of attractive interactions between the particles as well as a particle and the proximal protuberance is observed when the asymmetry is very small and the width at the stenosis throat is between two critical values. This force is weak for large asymmetry. When multiparticle suspensions with a hematocrit 0.2 are injected from the inlet, we find that there are two critical values $b_{c\Phi0}$ and $b_{c\Phi}$. Particles tend to gather near the centerline in the flat tube far away from the stenosis when $b < b_{c\Phi0}$ or $b > b_{c\Phi}$ and vice versa.

Although the numerical simulations are performed in two dimensions, some similar behavior is expected in three dimensions. It should be noted that there is a crucial difference. In the two-dimensional case, both the velocities of particles and those at all fluid nodes vanish when the throat is completely blocked by particles. There is space for the fluid to flow even if the particles are blocked by the stenosis throat in three dimensions. The simulations on the particle suspensions in three-dimensional symmetric stenotic arteries with the lattice Boltzmann method are undertaken with a PC cluster, which will be presented elsewhere.

[1] B. Das, P.C. Johnson, and A.S. Popel, Biorheology **35**, 1 (1998).

[2] R.E. Peveril, R.W. Harper, and J.J. Smolich, Int. J. Cardiol. **71**, 149 (1999).

[3] R. Mittal, S.P. Simmons, and H.S. Udaykumar, J. Biomech. Eng. **123**, 325 (2001).

[4] Jr. Buchanan, C. Kleinstreuer, and J.K. Comer, Comput. Fluids **29**, 695 (2000).

[5] J.S. Stround, S.A. Berger, and D. Saloner, J. Biomech. Eng. **124**, 9 (2002).

[6] Y.C. Fung, *Biomechanics Circulation* (Springer-Verlag, Berlin, 1997).

[7] G. Segré and A. Silberberg, Nature (London) **189**, 219 (1961).

[8] R. Fahraeus, Physiol. Rev. **9**, 241 (1929); J.H. Barbee and G.R. Cokelet, Microvasc. Res. **3**, 6 (1971).

[9] J. Feng, H.H. Hu, and D.D. Joseph, J. Fluid Mech. **277**, 271 (1994).

[10] C. Migliorini *et al.*, Biophys. J. **83**, 1834 (2002).

[11] J. Feng and S. Weinbaum, J. Fluid Mech. **422**, 281 (2000).

[12] G.R. McNamara and G. Zanetti, Phys. Rev. Lett. **61**, 2332 (1988).

[13] S. Chen, H. Chen, D.O. Martinez, and W.H. Matthaeus, Phys. Rev. Lett. **67**, 3776 (1991).

[14] Y.H. Qian, D. d'Humiéres, and P. Lallemand, Europhys. Lett. **17**, 479 (1992).

[15] X.W. Shan and X.Y. He, Phys. Rev. Lett. **80**, 65 (1998).

[16] S.Y. Chen and G.D. Doolen, Annu. Rev. Fluid Mech. **30**, 329 (1998).

[17] A.J.C. Ladd, J. Fluid Mech. **271**, 285 (1994).

[18] C.K. Aidun and Y. Lu, J. Stat. Phys. **81**, 49 (1995); C.K. Aidun, Y. Lu, and E. Ding, J. Fluid Mech. **373**, 287 (1998).

[19] D. Qi, J. Fluid Mech. **385**, 41 (1999).

[20] O. Behrend, Phys. Rev. E **52**, 1164 (1995).

[21] P. Raiskinmaki *et al.*, Comput. Phys. Commun. **129**, 185 (2000).

[22] D.R. Noble and J.R. Torczynski, Int. J. Mod. Phys. C **9**, 1189 (1998).

[23] T. Inamuro, K. Maeba, and F. Ogino, Int. J. Multiphase Flow **26**, 1981 (2000).

[24] H.P. Fang, Z.F. Lin, and Z.W. Wang, Phys. Rev. E **57**, R25 (1998).

[25] H.P. Fang, Z.W. Wang, Z.F. Lin, and M.R. Liu, Phys. Rev. E **65**, 051925 (2002).

[26] A.G. Hoekstra *et al.*, Lect. Notes Comput. Sci. **2657**, 997 (2003).

[27] M. Hirabayashi *et al.*, Phys. Rev. E **68**, 021918 (2003).

[28] H.P. Fang, D.R. Noble, H.H. Hu, and S.Y. Chen (unpublished).

[29] O. Filippova and D. Hanel, Comput. Fluids **26**, 697 (1997).

[30] R. Mei, L. Lou, and W. Shyy, J. Comput. Phys. **155**, 307 (1999).

[31] R.Z. Wan, H.P. Fang, Z.F. Lin, and S.Y. Chen, Phys. Rev. E **68**, 011401 (2003).

[32] P.L. Bhatnagar, E.P. Gross, and M. Krook, Phys. Rev. A **94**, 511 (1954).

[33] X. He and L-S. Luo, Phys. Rev. E **56**, 6811 (1997).

[34] T. Abe, J. Comput. Phys. **131**, 241 (1997).

[35] S.Y. Chen, D. Matinez, and R.W. Mei, Phys. Fluids **8**, 2527 (1996).

[36] Q. Zou and X. He, Phys. Fluids **9**, 1591 (1997).

[37] M.P. Allen and D.J. Tildesley, *Computer Simulation of Liquid* (Clarendon, Oxford, 1987).

[38] X. He and L. Luo, J. Stat. Phys. **88**, 927 (1997).

[39] Johns F. Douglas, Janusz M. Gasiorek, and John A. Swaffield, *Fluid Mechanics* (Longman Singapore, Singapore, 1995).

[40] A.J.C. Ladd Phys. Fluids **9**, 491 (1997).

[41] X.F. Yuan and R.C. Ball, J. Chem. Phys. **101**, 9016 (1994).

[42] H.B. Li and H.P. Fang (unpublished).

[43] J.C. Croker and D.G. Grier, Phys. Rev. Lett. **73**, 352 (1994); A.E. Larsen and D.G. Grier, Nature (London) **385**, 230 (1997).

[44] H.B. Li, X.Y. Lu, H.P. Fang, and Z.F. Lin (unpublished).

[45] K. To, P.Y. Lay, and H.K. Pak, Phys. Rev. Lett. **86**, 71 (2001).